

Graph state generation with noisy mirror-inverting spin chains

Stephen R Clark, Alexander Klein, Martin Bruderer and Dieter Jaksch

Clarendon Laboratory, University of Oxford, Oxford OX1 3PU, U.K.

E-mail: s.clark@physics.ox.ac.uk

Abstract. We investigate the influence of noise on a graph state generation scheme which exploits a mirror inverting spin chain. Within this scheme the spin chain is used repeatedly as an entanglement bus (EB) to create multi-partite entanglement. The noise model we consider comprises of each spin of this EB being exposed to independent local noise which degrades the capabilities of the EB. Here we concentrate on quantifying its performance as a single-qubit channel and as a mediator of a two-qubit entangling gate, since these are basic operations necessary for graph state generation using the EB. In particular, for the single-qubit case we numerically calculate the average channel fidelity and whether the channel becomes entanglement breaking, i.e., expunges any entanglement the transferred qubit may have with other external qubits. We find that neither local decay nor dephasing noise cause entanglement breaking. This is in contrast to local thermal and depolarizing noise where we determine a critical length and critical noise coupling, respectively, at which entanglement breaking occurs. The critical noise coupling for local depolarizing noise is found to exhibit a power-law dependence on the chain length. For two qubits we similarly compute the average gate fidelity and whether the ability for this gate to create entanglement is maintained. The concatenation of these noisy gates for the construction of a five qubit linear cluster state and a Greenberger-Horne-Zeilinger state indicates that the level of noise that can be tolerated for graph state generation is tightly constrained.

PACS numbers: 03.67.Mn, 03.67.Lx

1. Introduction

Entanglement appears to be a crucial ingredient for the potentially remarkable speedup of a quantum computer compared to that of a classical computer [1, 2]. This observation is especially highlighted within the one-way quantum computing model [3, 4]. Here the state of a quantum many-body system, typically composed of spin- $\frac{1}{2}$ or qubit subsystems, can serve a universal resource for quantum computing in which the computation is driven by successive von-Neumann measurements on the individual constituents. While the characterization of multipartite entanglement in a general quantum many-body state remains an open problem, initial states which can act as a universal resource for one-way quantum computing are within an increasingly well-studied class called *graph states* [5, 6].

Graph states are many-body quantum states which have an intuitive representation in terms of mathematical graphs. More precisely, vertices of a graph are assigned to the constituent qubits, each initialized in a state $|+\rangle = (|0\rangle + |1\rangle)/\sqrt{2}$, and edges connecting vertices represent a pattern of Ising-type interactions[‡] that have subsequently taken place between these qubits. In this way the graph describes a preparation procedure for this class of states, as depicted in figure 1(a). Within the graph formalism many of the properties of graph states, such as their Schmidt measure and robustness to noise, can be computed efficiently despite being intractable for a general state [5, 7, 6]. From such studies it is known that there are graph states that contain the maximum amount of entanglement permissible for any given number of qubits. As such, graph states form a highly non-trivial class of quantum states.

It is believed that some of the tremendous challenges faced in realizing a quantum computer can be lessened by using an architecture based on graph states [6]. In particular the underlying resource for one-way quantum computing is a special class of graph states, called cluster states [8], which are represented by graphs with a regular lattice geometry like that shown in figure 1(b). This pattern of nearest-neighbour Ising interactions is a geometry which is very naturally suited to quantum lattice systems. Additionally, by separating the preparation of entanglement from its consumption within a computation the one-way model can be arranged to accommodate lossy or even probabilistic processes during the preparation phase. Beyond cluster states more general graph states are also an efficient resource for *specific* quantum computations [4] and so represent a preferred experimental route to quantum information processing where qubits are a precious quantity. Graph states also play a prominent role as code-words in quantum error correction [9] which permit the reliable storage of quantum information in the presence of noise.

There are now a diverse range of proposals for the preparation of graph states in realistic physical systems [6]. These include the direct use of linear optics and photon resolving measurements to construct graph states with photons via a non-deterministic protocol [10]. As a proof of principle an entirely optical creation of a 4 qubit graph state was recently realized and used to implement a 2 qubit Grover search algorithm [11]. Other frameworks include using hybrid systems which combine optical and solid state qubits [12]. Another method is to instead engineer a many-body quantum system whose ground state is a graph state so that beyond engineering the nearest-neighbour interactions the preparation becomes a cooling problem [13]. The approach which we consider in this paper is based on exploiting a spin chain

[‡] This Ising interaction is typically taken to implement a *controlled phase* or $c\text{-}\sigma^z$ gate.

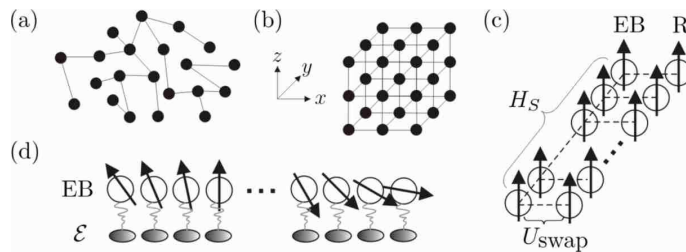


Figure 1. (a) An arbitrary graph state. (b) A 3D cluster state. (c) The spin-ladder arrangement used in the graph state generation scheme. One leg of the ladder is the EB spin chain with a mirror inverting Hamiltonian H_S . The other is a chain of decoupled spins which form a storage register R. Coupling between adjacent spins in EB and R is dynamically controlled to implement a rapid swap gate U_{swap} . (d) The EB spin chain with each spin exposed to an independent local environment \mathcal{E} .

with fixed engineered couplings chosen such that its dynamical evolution is mirror inverting [14, 15, 16]. Such spin chains have attracted much attention because of their ability to perform perfect state transfer and therefore act as a quantum communication channel [17, 18, 19, 20]. In reference [21] it was shown that mirror inverting spin chains are capable of implementing a specific type of multi-qubit circuit that is naturally suited to the generation of entanglement of the type present in graph states. For this reason we call this type of chain an *entangling bus* (EB). When the EB is used within a spin-ladder arrangement, as shown in figure 1(c) where the second leg of the ladder is a register R of qubits, it permits the efficient generation of arbitrary graph states within this register.

Experimental realizations of quantum systems inevitably possess a coupling to a surrounding environment composed of a large number of degrees of freedom which are beyond the experimenters control [22]. This coupling introduces quantum noise that destroys quantum coherence of the system (i.e. decoherence). This is broadly classified as dissipation, when accompanied by the exchange of energy between the system and environment, or dephasing when there is no energy exchange. The effects of noise on a spin chain used as quantum channels has been investigated previously [23, 24, 25, 26]. Here we consider a broader set of properties including the ability of mirror inverting chains to both distribute and generate entanglement which are crucial for the more challenging use of them as EB. To do this we consider a specific, but physically relevant [27, 7], noise model where each spin in the EB is weakly coupled to an independent environment \mathcal{E} and the complete chain is described by a master equation, as illustrated in figure 1(d).

This paper is organized as follows. In section 2 mirror inversion in spin chains is thoroughly described. In section 3 the graph state generation scheme exploiting mirror inversion is briefly reviewed. Section 4 outlines the methods we apply to characterize the performance of the EB as a single-qubit channel and as a two-qubit gate in the presence of noise. In section 5 the class of local noise that is considered in this work is introduced. The influence of these local noise models are then systematically analyzed in section 7 for both the single-qubit channel and two-qubit gate scenario. For the readers convenience the detailed results of section 7 are summarized in its first subsection. We then examine the implications of these results for the generation of a

five qubit linear cluster state and Greenberger-Horne-Zeilinger (GHZ) state in section 8 before concluding in section 9.

2. Mirror-inverting spin chains

Our starting point is a spin- $\frac{1}{2}$ chain composed of N spins which is governed by an XX Hamiltonian of the form (taking $\hbar = 1$)

$$H_S = -\frac{J}{2} \sum_{j=1}^{N-1} t_j (\sigma_j^x \sigma_{j+1}^x + \sigma_{j+1}^y \sigma_j^y) + \frac{1}{2} \sum_{j=1}^N h_j (\mathbb{1} - \sigma_j^z), \quad (1)$$

with spatially dependent spin couplings t_j and local fields h_j . We denote the σ^z basis states of the chain as $|q_1, \dots, q_N\rangle$ with $q_j \in \{0, 1\}$ representing \uparrow and \downarrow respectively. Since $[H_S, \mathbb{N}] = 0$, where $\mathbb{N} = \frac{1}{2} \sum_{j=0}^N (\mathbb{1} - \sigma_j^z)$ §, then H_S is block-diagonal with respect to subspaces \mathcal{H}_n spanned by states $|q_1, \dots, q_N\rangle$ with $\sum_j q_j = n$. The spin chain Hamiltonian H_S can be mapped to a 1D spinless fermionic lattice model using the Jordan-Wigner transformation (JWT) [28] giving

$$H_F = -J \sum_{j=1}^{N-1} t_j (c_j^\dagger c_{j+1} + c_{j+1}^\dagger c_j) + \sum_{j=1}^N h_j c_j^\dagger c_j,$$

and subsequently diagonalized into an explicitly free-fermion bi-linear form

$$H_D = \sum_{k=1}^N \epsilon_k a_k^\dagger a_k,$$

with spectrum ϵ_k . Here both $c_j^\dagger(c_j)$ and $a_k^\dagger(a_k)$ are fermionic creation (annihilation) operators, obeying the usual anticommutation relation, associated to lattice site j and the energy eigenstate k respectively. Under this mapping $\mathbb{N} = \sum_j c_j^\dagger c_j$ and the subspaces \mathcal{H}_n it defines are identified with the fermion number. The fermion vacuum is then $|\text{vac}\rangle = |0, \dots, 0\rangle$ with energy $E_{\text{vac}} = 0$ and spin states $|q_1, \dots, q_N\rangle$ become n fermion Fock states $|q_1, \dots, q_N\rangle \mapsto (c_1^\dagger)^{q_1} \dots (c_N^\dagger)^{q_N} |\text{vac}\rangle$ with the operator ordering following the lattice numbering. We denote the blocks of H_F acting on subspaces \mathcal{H}_n as $H_F^{(n)}$ and since H_F is a non-interacting Hamiltonian its properties are entirely defined by its single-particle Hamiltonian $H_F^{(1)}$.

To be mirror inverting all localized states $|j\rangle = c_j^\dagger |\text{vac}\rangle$ in \mathcal{H}_1 are required to evolve after a given fixed time τ under $H_F^{(1)}$ into the localized state $|\bar{j}\rangle$ (up to a phase) where $\bar{j} = N - j + 1$ is the mirror location in the lattice. While this places constraints on the couplings t_j and fields h_j there are still an infinite number of permissible choices [17, 18]. In this work we exclusively consider the simplest and fastest mirror inverting couplings [19] where $t_j = \frac{1}{2} \sqrt{j(N-j)}$ and $h_j = h$. With this choice $H_F^{(1)}$ takes the form $H_F^{(1)} = -JS_x + h$ where S_x is the x -axis angular momentum operator for a spin- \mathcal{S} pseudo-particle where $\mathcal{S} = \frac{1}{2}(N-1)$. Localized $n = 1$ states are then identified with S_z eigenstates $\{|\mathcal{S}, l\rangle_z\}$ of the pseudo-spin through the ordering $|1\rangle = |\mathcal{S}, -\mathcal{S}\rangle_z, \dots, |N\rangle = |\mathcal{S}, \mathcal{S}\rangle_z$. If we now consider the time evolution in \mathcal{H}_1 for a time $\tau = \pi/J$ we see that $U^{(1)} = \exp(-iH_F^{(1)}\tau) = \exp(-ih\pi/J) \exp(i\pi S_x)$ is a rotation of the pseudo-spin by π about its x -axis and is therefore equivalent to the

§ The operator \mathbb{N} counts the number of spins which are \downarrow .

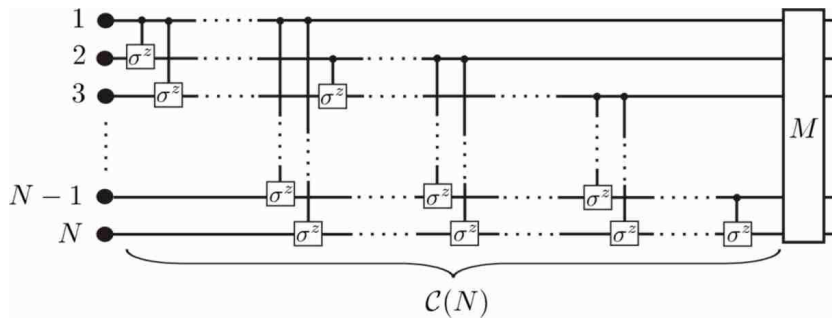


Figure 2. The quantum circuit $\mathcal{C}(N)$ composed of $c\text{-}\sigma^z$ gates between all distinct pairs of qubits obtained by evolving the mirror-inverting spin chain with Hamiltonian H_S for a time τ .

mirror inversion of a single fermion in the lattice [14, 15]. Interestingly, we note that similar effects also take place in a chain of coupled harmonic oscillators as discussed in reference [29].

Moving our consideration back to the full state space of the lattice it follows that the localized modes c_j^\dagger are related to the energy eigenmodes a_k^\dagger via irreducible representations $d_{jk}(\frac{\pi}{2})$ of a $\pi/2$ rotation about the y -axis of the pseudo-spin [30] as $a_k^\dagger = \sum_j d_{jk}(\frac{\pi}{2}) c_j^\dagger$. The angular momentum couplings also result in the spectrum of H_D being linear as $\epsilon_k = J(k - \mathcal{S} - 1) + h$ over the range $\epsilon_k \in [-\mathcal{S} + h, \mathcal{S} + h]$, and so in order to ensure that the state $|\text{vac}\rangle$ is the non-degenerate ground state of the system, for all J , we require $h > \mathcal{S}J$. We can define the many-body gap between the vacuum ground state and the first excited state as Δ giving $h = \mathcal{S}J + \Delta$ and for $\Delta > 0$ the first excited state is always in the \mathcal{H}_1 subspace. Note also that with this definition in the limit $J \rightarrow 0$ we have that Δ is the local gap for each decoupled spin. Additionally, we can choose Δ/J as an even number such that mirror inversion proceeds with no phase modulo 2π .

The mirror inverting dynamics in \mathcal{H}_1 is equivalent to the transformation $U c_j^\dagger U^\dagger = c_j^\dagger$ on the localized modes with $U = \exp(-iH_F\tau)$. Applying this evolution to an arbitrary n fermion Fock state, and performing the inverse JWT, mirror inversion results in

$$e^{-iH_F\tau} |q_1, \dots, q_N\rangle = e^{-i\pi\Sigma_n} |q_N, \dots, q_1\rangle, \quad (2)$$

where $\Sigma_n = \frac{1}{2}n(n-1)$ is the number of anti-commutations of the operators c_j^\dagger required to reestablish the correct ordering. The simplest utilization of mirror inversion is state transfer where we restrict our consideration to the subspace $\mathcal{H}_0 \oplus \mathcal{H}_1$ spanned by the spin-polarized state $|\text{vac}\rangle$ and the single spin-flip states $|j\rangle$. We then encode an input qubit as a superposition $|\psi\rangle = \nu_0 |\text{vac}\rangle + \nu_1 |1\rangle$ using the first spin in the chain and under purely coherent evolution this state is transferred perfectly to the last spin as $|\psi\rangle = \nu_0 |\text{vac}\rangle + \nu_1 |N\rangle$ [14, 15]. The same conclusion follows trivially for a mixed input state.

A more general use of mirror inversion follows from noting that the phase $\pi\Sigma_n$ in equation (2) is non-linear in n and only appears between subspaces with different fermion number for $n \geq 2$. Thus for input states of the chain which involve superpositions spanning several multi-particle subspaces these phases will

create entanglement in the mirror-inverted output state [21, 17]. More precisely, the evolution U of the chain for a time τ is equivalent to a quantum circuit $\mathcal{C}(N)$ composed of $c\text{-}\sigma^z$ gates between all distinct pairs of N qubits followed by the inversion operator M , as shown in figure 2. This circuit has the useful property that if any $N - q$ spins in the chain are in the state $|0\rangle$, then this circuit reduces to $\mathcal{C}(q)$ between the remaining q qubits, independent of their locations, followed by the full inversion M of the chain.

3. Graph state generation with an engineered spin ladder

Here we briefly review the scheme given in [21] where the general multi-qubit circuit $\mathcal{C}(N)$ implemented by a mirror inverting chain is exploited to construct graph states. This is achieved by considering a spin-ladder with a *comb*-like arrangement of couplings as depicted in figure 1(c). One chain of the ladder possess fixed mirror inverting couplings and forms the EB, while the other chain is composed of decoupled spins forming the register R. We assume that spins in the register can be individually manipulated and measured. Dynamical control of the spin couplings is restricted to those between adjacent spins in the EB and R where we require the ability to rapidly implement a swap gate. In this way entanglement generation is achieved by repeatedly swapping qubits between R and EB and thereby using the quantum circuit $\mathcal{C}(N)$.

The entire spin ladder is taken to be initialized in a spin polarized state. The scheme begins by choosing a set of register spins G that will be the graph qubits, and transforming all of them to $|+\rangle$. For any subset $Q \subset G$ of graph qubits which are transferred into the EB and evolved for a time τ the resulting circuit $\mathcal{C}(|Q|)$ will apply $c\text{-}\sigma^z$ gates between all of the corresponding graph vertices. In the case where two graph qubits in the set Q do not already possess an edge between them this process will establish one, otherwise it will remove the edge. By proceeding iteratively we can induce any pattern of edges between the graph qubits G . Starting with $g = 1$, we

- (i) transfer the g -th graph qubit from G , and all graph qubits $g_c > g$ which are required to connect to g , as specified by the graphs adjacency matrix Γ , into the EB;
- (ii) allow the EB to evolve for a time τ and create a complete set of connections between all these previously unconnected vertices;
- (iii) then transfer qubit g back to the register while leaving the qubits g_c to evolve for one cycle longer in the EB, subsequently removing all the connections between them;
- (iv) finally the qubits g_c are transferred back to the register and step (i) is repeated with $g \mapsto g + 1$.

Thus, any graph with n vertices can be generated in at most $O(2n)$ uses of the EB in contrast to $O(n^2)$ steps if the EB was used to implement single $c\text{-}\sigma^z$ gates only. Although the EB has a linear topology, by using this method any two qubits in the register can be entangled thereby allowing for arbitrary topologies of the graph state. To avoid overlap between EB and register graph qubits after inversion one may choose $|G| \leq \lceil N/2 \rceil$ with locations in the first half of the register.

4. Characterizing a noisy spin-chain

The main aim of this work is to characterize the effect of noise on the performance of the EB and determine its implications for using the EB within the graph state generation scheme. For simplicity we determine the performance of the EB at implementing its two most basic operations, namely acting as a single-qubit quantum channel and as a mediator of a two-qubit $c\text{-}\sigma^z$ gate. These represent the minimal operations required for the EB to be used for graph state generation. For this reason we consider the effect of noise only on the EB spin chain and not the register R. Additionally we focus on the scenario in which the input and output qubits are the end spins of the EB. Before describing any specifics about the noise we first outline some general theoretical tools which provide insightful measures of performance.

4.1. Average fidelity

Suppose we have a system which, when no noise is present, performs a particular unitary operation U . With the inclusion of noise the action of the system is instead described by a superoperator Λ . How close the noisy operation remains to U for a particular initial pure state $|\psi\rangle \in \mathbb{C}^{\text{d}}$ can be quantified by the fidelity [31]

$$F(\psi) = \langle \psi | U^\dagger \Lambda\{|\psi\rangle\langle\psi|\} U | \psi \rangle. \quad (3)$$

The overall performance of the noisy system at implementing U can then be measured by the average of this fidelity over all possible initial pure states

$$\langle F \rangle = \int_{S^{2\text{d}-1}} F(\psi) \text{d}\psi,$$

where integration is over the unit sphere $S^{2\text{d}-1}$ in \mathbb{C}^{d} and $\text{d}\psi$ is the normalized measure on the sphere, also known as a Haar measure. For the case of a single qubit this is equivalent to integration over the Bloch sphere as $\int_{S^3} \text{d}\psi = \frac{1}{4\pi} \int_{-\pi}^{\pi} \text{d}\phi \int_0^{\pi} \text{d}\theta \sin(\theta)$. Now given a Kraus decomposition of the superoperator Λ as

$$\Lambda\{\rho\} = \sum_{m=1}^{\text{d}^2} A_m \rho A_m^\dagger,$$

where A_m are Kraus operators there is a compact formula for $\langle F \rangle$ in any dimension d . Firstly, we form a new superoperator \mathcal{E} with Kraus operators $E_m = A_m U^\dagger$, such that $\mathcal{E}\{U\rho U^\dagger\} = \Lambda\{\rho\}$, which describes exclusively the effect of noise. It can then be shown [32, 33] that

$$\langle F \rangle = \frac{1}{\text{d}(\text{d}+1)} \left(\sum_{m=1}^{\text{d}^2} |\text{tr}(E_m)|^2 + \text{d} \right). \quad (4)$$

We exploit this formula to determine the single qubit channel (or $\mathbb{1}$ operation) fidelity, and the gate fidelity for the effective $c\text{-}\sigma^z$ operation between two qubits achieved with a noisy EB.

4.2. Entanglement breaking and generation

While the average fidelity provides a quantitative measure of a noisy operation, a more qualitative way of characterising the severity of the noise is to determine whether

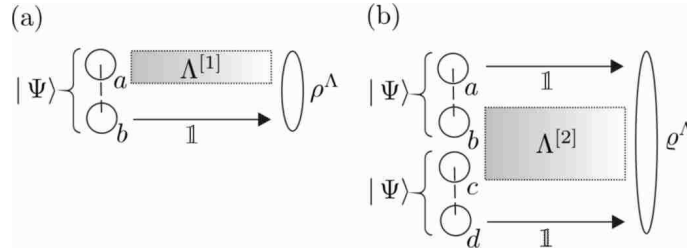


Figure 3. A schematic representation of the Jamiolkowski isomorphism used to characterize a superoperator (a) $\Lambda^{[1]}$ acting on a single subsystem and (b) $\Lambda^{[2]}$ acting on a pair of subsystems in the maximally entangled state $|\Psi\rangle$ (see Appendix C for details), as quantum states ρ^Λ and ϱ^Λ respectively.

the corresponding superoperator $\Lambda^{[1]}$, which acts on one subsystem, preserves any entanglement that the subsystem has with other external systems. Quite generally if $\Lambda^{[1]}$ acts on the subsystem b , with Hilbert space $\mathcal{H}_b = \mathbb{C}^{\mathfrak{d}_b}$, it is described as *entanglement breaking* [7] if the final state $\rho_{ab}^{\text{out}} = \mathbb{1}_a \otimes \Lambda_b^{[1]}\{\rho_{ab}^{\text{in}}\}$ is separable for every (possibly entangled) initial state ρ_{ab}^{in} of the composite system of b and another subsystem a with Hilbert space $\mathcal{H}_a = \mathbb{C}^{\mathfrak{d}_a}$. Becoming entanglement breaking therefore signifies that the channel can no longer be used to distribute entanglement.

Remarkably, for a single-qubit ($\mathfrak{d}_b = 2$) the PPT criterion [34, 35] (see Appendix B) in combination with the Jamiolkowski isomorphism [36] (see Appendix C and figure 3) give a straightforward condition for $\Lambda^{[1]}$ to be entanglement breaking. Firstly, it is sufficient to compute the state ρ^Λ from the Jamiolkowski isomorphism (see figure 3(a)), where $\mathfrak{d}_a = \mathfrak{d}_b = 2$, since this contains all the properties of $\Lambda^{[1]}$. It then follows that $\Lambda^{[1]}$ is entanglement breaking (for any \mathfrak{d}_a) if and only if the state ρ^Λ is separable since this implies that $\Lambda^{[1]}$ has a Kraus representation composed entirely of projectors. Finally, since ρ^Λ is a two qubit state its separability follows directly from the PPT criterion. The entanglement breaking characteristics of the EB when acting as a single-qubit channel are of importance since the graph state generation scheme involves its successive use. We therefore have a minimum requirement that for the EB to be useful it must, at the very least, preserve any entanglement that an input qubit may have with other external qubits, such as those in the register, when acting purely as a quantum channel. This then provides an essential, albeit optimistic, bound to its tolerance for noise.

When the evolution of two subsystems is described by a superoperator $\Lambda^{[2]}$ it is clearly of interest to determine when this evolution is capable of generating entanglement between these subsystems \parallel . Specifically, for $\rho_{bc}^{\text{out}} = \Lambda_{bc}^{[2]}\{\rho_{bc}^{\text{in}}\}$ we may ask when is ρ_{bc}^{out} always separable for all possible separable initial state ρ_{bc}^{in} ? This implies that the superoperator $\Lambda^{[2]}$ never generates entanglement. The question can be answered by again appealing to the Jamiolkowski isomorphism via the state ϱ^Λ associated to $\Lambda^{[2]}$. It follows that $\Lambda^{[2]}$ is of product form $\Lambda_{bc}^{[2]} = \Lambda_b^{[1]} \otimes \Lambda_c^{[1]}$ and incapable of generating entanglement if its corresponding state ϱ^Λ is separable with respect to the bipartition of the system as $(ab)(cd)$ as in figure 3(b). Thus the property of *entanglement generation* can also be phrased as a state separability problem. For two qubits ($\mathfrak{d}_a = \mathfrak{d}_b = 2$) the mixed state ϱ^Λ describes four qubits. In this case the

\parallel When this results in an entangled mixed state it can then, in principle, be distilled.

PPT criterion only provides a necessary condition for the $(ab)(cd)$ separability of this state. Thus the PPT criterion can only determine a point at which we can no longer be certain whether $\Lambda^{[2]}$ can generate entanglement. Nonetheless this point provides a quantitative cut-off which should be avoided if the noisy entangling operation is to be of practical use.

5. Noise models

We consider noise which is described by a quantum master equation of Lindblad form

$$\frac{\partial}{\partial t}\rho(t) = -i[H_S, \rho(t)] + \mathcal{L}\{\rho(t)\}, \quad (5)$$

where $\mathcal{L}\{\cdot\}$ is the Lindbladian describing the incoherent contribution to the evolution of the density matrix $\rho(t)$. The microscopic derivation of such a master equation relies on the Born-Markov approximation and is typically found to be accurate for systems with a weak coupling to a much larger environment [22].

We consider a subclass of this noise model where each spin experiences an independent local environment so the Lindbladian decomposes as a sum $\mathcal{L}\{\cdot\} = \sum_j \mathcal{L}_j\{\cdot\}$. We make one further restriction and consider the local Lindbladian $\mathcal{L}_j\{\cdot\}$ to be of a physically well motivated form commonly encountered in quantum optical problems after applying the rotating wave approximation [27, 7]. Specifically,

$$\begin{aligned} \mathcal{L}_j\{\rho(t)\} = & \frac{\alpha}{2} [2\sigma_j^- \rho(t)\sigma_j^+ - \sigma_j^+ \sigma_j^- \rho(t) - \rho(t)\sigma_j^+ \sigma_j^-] \\ & + \frac{\beta}{2} [2\sigma_j^+ \rho(t)\sigma_j^- - \sigma_j^- \sigma_j^+ \rho(t) - \rho(t)\sigma_j^- \sigma_j^+] \\ & + \frac{\gamma}{2} [\sigma_j^z \rho(t)\sigma_j^z - \rho(t)], \end{aligned} \quad (6)$$

where α , β and γ are the rates for jumps $|\uparrow\rangle \rightarrow |\downarrow\rangle$, $|\downarrow\rangle \rightarrow |\uparrow\rangle$, and pure dephasing, respectively. To give an overview of the physics contained in this model let us consider the situation where $J = 0$ in H_S , defined in equation (1), so each spin decouples with a local Hamiltonian of the form $H_j = \frac{\Delta}{2}(\mathbb{1} - \sigma_j^z)$. If we move to the interaction picture of H_j for each spin \blacksquare it is readily found that the evolution of the j -th spin is described by $\tilde{\rho}(t) = e^{\mathcal{L}_j t}\{\tilde{\rho}\}$ with \mathcal{L}_j remaining in terms of the untransformed operators in equation (6) due to phase cancellation. We now write the initial state $\tilde{\rho}$ as

$$\tilde{\rho} = \frac{1}{2} [\mathbb{1} + \langle\tilde{\sigma}_x\rangle\tilde{\sigma}_x + \langle\tilde{\sigma}_y\rangle\tilde{\sigma}_y + \langle\sigma_z\rangle\sigma_z],$$

from which the general solution is found to be [27]

$$\begin{aligned} e^{\mathcal{L}t}\{\rho\} = & \frac{1}{2} \left[\mathbb{1} + \langle\sigma_z\rangle_s \sigma_z + e^{-\frac{1}{2}(\alpha+\beta+2\gamma)t} (\langle\tilde{\sigma}_x\rangle\tilde{\sigma}_x + \langle\tilde{\sigma}_y\rangle\tilde{\sigma}_y) \right. \\ & \left. + e^{-(\alpha+\beta)t} (\langle\sigma_z\rangle - \langle\sigma_z\rangle_s)\sigma_z \right]. \end{aligned}$$

As is well known this solution shows exponential convergence with rate $\alpha + \beta$ of $\langle\sigma_z(t)\rangle$ to its stationary ($t \rightarrow \infty$) value of $\langle\sigma_z\rangle_s = \frac{\beta - \alpha}{\alpha + \beta}$ and the exponential decay, with rate $\frac{1}{2}(\alpha + \beta + 2\gamma)$, of the coherences $\langle\tilde{\sigma}_\pm(t)\rangle$ to their stationary value $\langle\sigma_\pm\rangle_s = 0$. The general solution to this noise model can be expressed in a Kraus form [31] with Kraus

\blacksquare We shall denote the interaction picture of a Hamiltonian H by a tilde as $\tilde{O} = e^{iHt} O e^{-iHt}$.

operators

$$\begin{aligned} E_1 &= \begin{pmatrix} \Upsilon_1 & 0 \\ 0 & \Upsilon_2 \end{pmatrix}, & E_2 &= \sqrt{P_\uparrow} \begin{pmatrix} 0 & \sqrt{1 - e^{-(\alpha+\beta)t}} \\ 0 & 0 \end{pmatrix}, \\ E_3 &= \begin{pmatrix} \Upsilon_3 & 0 \\ 0 & \Upsilon_4 \end{pmatrix}, & E_4 &= \sqrt{P_\downarrow} \begin{pmatrix} 0 & 0 \\ \sqrt{1 - e^{-(\alpha+\beta)t}} & 0 \end{pmatrix}, \end{aligned} \quad (7)$$

where $P_\uparrow = \frac{\beta}{\alpha+\beta}$, $P_\downarrow = \frac{\alpha}{\alpha+\beta}$ are the stationary spin populations and Υ_i are functions of α, β and γ which we give explicitly in Appendix A. We also show in Appendix A that this noise model reduces to a number of well known and simpler models in specific limits. In particular, if we parameterize the rates as (taking Boltzmann's constant $k_B = 1$)

$$\alpha(T) = \kappa \frac{e^{-\Delta/T}}{(1 + e^{-\Delta/T})} \quad \text{and} \quad \beta(T) = \kappa \frac{1}{(1 + e^{-\Delta/T})} \quad (8)$$

for an arbitrary γ , we obtain a total decay rate $\alpha(T) + \beta(T) = \kappa$ that is independent of T . In this case the stationary density matrix $\rho_s = \lim_{t \rightarrow \infty} \rho(t)$ for the spin is equivalent to a thermal state of temperature T . Consequently in this regime the master equation describes *finite-temperature* noise caused by the coupling to a generic thermal reservoir at temperature T local to each spin. At $T = 0$ and $\gamma = 0$ we have $\alpha = 0$ and $\beta = \kappa$ which describes *decay* noise. For $T \rightarrow \infty$ we have $\alpha = \beta = \frac{1}{2}\kappa$ and after setting $\gamma = \frac{1}{2}\kappa$, so the populations and coherences decay at the same rate, this results in *depolarizing* noise. Taking $\alpha = \beta = 0$ and $\gamma = \kappa$ we obtain pure *dephasing* noise. We shall consider each of these limiting cases as local noise in the EB.

If we now consider this class of noise in the context of a single-qubit channel we can determine the properties which were outlined in section 4. Indeed using the Kraus operators in equation (7) the average fidelity of the channel can be computed via equation (4) and is given in full in Appendix A. The channel can be shown to become entanglement breaking if and only if the following condition is satisfied [7]

$$2P_\uparrow P_\downarrow e^{2\gamma t} \{\cosh([\alpha + \beta]t) - 1\} \geq 1. \quad (9)$$

In particular this result immediately indicates that, regardless of γ , whenever $\alpha = 0$ or $\beta = 0$ the channel is never entanglement breaking for finite coupling κ and times t since either $P_\downarrow = 0$ or $P_\uparrow = 0$, respectively. This result similarly holds when both $\alpha = 0$ and $\beta = 0$, giving a pure dephasing channel⁺, since we have $\cosh([\alpha + \beta]t) - 1 = 0$. In contrast a finite temperature channel (for any γ) can always become entanglement breaking for a finite κ and t . For $\gamma = 0$ this entanglement breaking occurs for a coupling

$$\kappa_c \geq \frac{J}{\pi} \cosh^{-1} \left[\frac{(1 + e^{-\Delta/T})^2}{2e^{-\Delta/T}} + 1 \right], \quad (10)$$

taking $t = \tau$, and this saturates at $\kappa_c \approx 0.56 J$ for $T \rightarrow \infty$. The presence of dephasing reduces this threshold. An important special case is where $\gamma = \frac{1}{2}\kappa$ which in the $T \rightarrow \infty$ limit gives a depolarizing channel with a threshold $\kappa_c \geq \frac{J}{\pi} \log(3) \approx 0.35 J$.

6. Numerical method

The numerical calculations we perform in this work is restricted to the class of 1D quantum lattice systems described by a master equation which include a Hamiltonian

⁺ Note in the case of pure dephasing the definitions of P_\uparrow and P_\downarrow in terms of α and β are meaningless and the stationary populations follow from the arbitrary initial state.

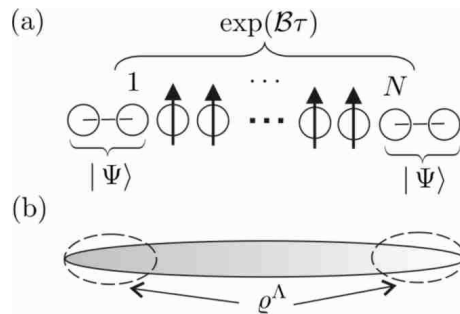


Figure 4. The setup used in numerical calculations to determine the effective two qubit superoperator $\Lambda^{[2]}$ of a noisy mirror-inverting chain. (a) Following the Jamiolkowski isomorphism the initial state ρ is a spin-polarized chain $|0\cdots 0\rangle$ aside from the end spins which are in maximally entangled states $|\Psi\rangle$ with corresponding ancillary spins. The spins $1, \dots, N$ in the chain are then evolved for a time τ while being exposed to noise. The total dynamical evolution of the chain is then described by the superoperator $\exp(\mathcal{B}\tau)$ which is the formal solution to equation (5). (b) The state ρ^Λ corresponding to $\Lambda^{[2]}$ is then extracted from the overall final state $\exp(\mathcal{B}\tau)\{\rho\}$ by tracing out all but the end spin pairs.

and a Lindbladian that are both composed of terms involving at most nearest-neighboring sites. It can be seen that both H_S and \mathcal{L} introduced in section 5 satisfy this constraint. The real time evolution for this class of master equation can be computed efficiently and to near-exact precision for systems composed of many sites using the mixed-state version of the Time Evolving Block Decimation (TEBD) algorithm [37, 2, 38]. We refer the reader to the literature for a detailed description of this method and note here only that for the calculations presented we found that a truncation parameter [38] up to $\chi = 20$ was sufficient. In figure 4 we depict the type of numerical calculation we have performed with this algorithm. These are based on the Jamiolkowski isomorphism which for two qubits requires the spin chain to be initialized in a pure state $|\Psi\rangle \otimes |0\cdots 0\rangle \otimes |\Psi\rangle$ with the two end spins being in a maximally entangled state $|\Psi\rangle = (|00\rangle + |11\rangle)/\sqrt{2}$ with corresponding ancillary spins shown in figure 4(a). We then use TEBD to time evolve the spins $1, \dots, N$ in the chain in the presence of noise and finally compute the reduced density matrix ρ^Λ of the two ancillary spins and the two end spins of the chain as depicted in figure 4(b). The state ρ^Λ then completely characterizes the accumulative noisy operation of the chain $\Lambda^{[2]}$ for two qubits.

7. Results

7.1. Summary of results

Having introduced all the necessary concepts we now investigate the influence of local decay, dephasing, thermal and depolarizing noise on the performance of the EB spin chain. We distinguish between two scenarios, namely where only one qubit is transferred into the spin chain so it acts as a quantum channel, and where two qubits are swapped into the chain such that the mirror inversion performs a $c\text{-}\sigma^z$ gate. We summarise the main results here and refer the reader to the proceeding subsections for more details.

When used as a single-qubit channel we find that neither local decay or dephasing noise become entanglement breaking. For local decay noise we find that the accumulative noise $\Lambda^{[1]}$ of the chain is identical to the local decay noise on any single spin and is therefore entirely independent on the chain length N . We show this useful property is a consequence of commuting coherent and dissipative contributions to the dynamics which is unique to local decay noise. The EB chain is found to be the most robust to local decay noise and is able to maintain $\langle F \rangle \geq 0.99$ for state transfer when $\kappa/J \leq 9.7 \times 10^{-3}$. The case of local dephasing noise is shown to be well modelled by a quantum channel subject to the same local dephasing noise along with a length dependent decay noise. For spin chains of lengths up to $N = 50$ the average fidelity remains above 99% as long as the dephasing noise fulfils $\kappa/J \leq 5 \times 10^{-3}$.

In contrast to these types of noise we find that local depolarizing and thermal noise become entanglement breaking for certain parameter regimes, for which analytical estimates are given. We further find that the length independence observed for the $T = 0$ local decay noise persists as a very weak length dependence for significant non-zero temperatures $T \leq 0.2\Delta$. For the local depolarizing noise we find that the critical coupling at which entanglement breaking occurs for a given chain length N is described by a power law $\kappa_c/J \approx N^{-x}$ with $x = 0.68$. This behaviour appears to be a consequence of the competition between the speed and spreading of a spin-packet in the chain. As expected the chain is most severely affected by local depolarizing noise with $\langle F \rangle \geq 0.99$ only for $\kappa/J < 3 \times 10^{-4}$ and lengths up to $N = 50$, which is more than an order of magnitude smaller than for local decay or dephasing noise.

For the two-qubit case we find that the average gate fidelity with local decay noise does not depend on the length N and remains above 99% for couplings below $\kappa/J \leq 4 \times 10^{-3}$. For thermal noise we find that $\langle F \rangle$ only depends very weakly on N as long as $T < 0.2\Delta$, as was the case a single-qubit. However, in contrast to the single-qubit case, this length independence in $\langle F \rangle$ does not extend to the accumulative noise $\Lambda^{[2]}$ superoperator itself. Both local dephasing and depolarizing noise have average gate fidelities which depend on N and for up to $N = 12$ spins the coupling is restricted to $\kappa/J \leq 2.5 \times 10^{-3}$ and $\kappa/J \leq 4 \times 10^{-4}$ in order for $\langle F \rangle > 0.99$. This again indicates that local depolarizing noise has the most severe influence and explains why its accumulative noise is well approximated by product noise.

7.2. Single-qubit channel

In this section we consider the EB as a single-qubit channel and systematically compute the average channel fidelity $\langle F \rangle$ and the minimum eigenvalue ϵ_{\min} of the partial transposition of the mixed state ρ^Λ that is isomorphic to accumulative noise of the chain $\Lambda^{[1]}$. From the PPT criterion this noise is entanglement breaking whenever $\epsilon_{\min} > 0$. We also use the behaviour of $\langle F \rangle$ over a wide parameter range to fit the noise $\Lambda^{[1]}$ of the chain to the specific class of single-spin noise introduced in section 5 and find that such fits are possible to very good accuracy.

7.2.1. Decay noise (low- T limit) - As was noted in reference [24], we find from our numerics that $\langle F \rangle$ displays no dependence on the length of the chain. Here we show that this unexpected feature is in fact a consequence of a much stronger result; specifically, the superoperator $\Lambda^{[1]}$ itself, which characterises the accumulative noise of the chain, is independent of N . This result implies that $\Lambda^{[1]}$ for any N is equivalent to $\Lambda^{[1]}$ for a chain with $N = 1$. Since a $N = 1$ chain is a single-qubit decay channel,

this allows us to conclude that state-transfer in a mirror-inverting chain with local decay noise is never entanglement breaking. Additionally, the coupling at which the fidelity drops to $\langle F \rangle < 0.99$ is found to be $\kappa_f/J = 9.7 \times 10^{-3}$, independent of N .

We now explain the independence of chain length observed. To begin we take a spin chain composed of N spins and a general Hamiltonian H_s satisfying $[H_s, \mathbb{N}] = 0$ so H_s is block diagonal with blocks $H_s^{(n)}$ in each subspace \mathcal{H}_n . Then we restrict our considerations to initial states of the chain $\rho(0)$ whose support is entirely contained in the subspace $\mathcal{H}_0 \oplus \mathcal{H}_1$. Evolution due to H_s and local decay noise has the convenient feature that the support of the state $\rho(t)$ at any time will also remain entirely within $\mathcal{H}_0 \oplus \mathcal{H}_1$. Consequently, we may project the full master equation of the chain into this subspace yielding

$$\frac{\partial}{\partial t} \rho(t) = -_1[H_s^{(0)} \oplus H_s^{(1)}, \rho(t)] + \frac{\kappa}{2} (2 P_1(t) \mathbb{P}_0 - \mathbb{P}_1 \rho(t) - \rho(t) \mathbb{P}_1).$$

Here $P_1(t) = \text{tr}(\mathbb{P}_1 \rho(t) \mathbb{P}_1)$ is the probability of being in the \mathcal{H}_1 subspace, with \mathbb{P}_0 and \mathbb{P}_1 being the projectors onto the subspaces \mathcal{H}_0 and \mathcal{H}_1 , respectively. If this projected master equation is expressed as $\dot{\rho}(t) = \mathbb{H}\{\rho(t)\} + \mathbb{L}\{\rho(t)\}$, where \mathbb{H} and \mathbb{L} are the coherent and dissipative superoperators, it follows that $[\mathbb{H}, \mathbb{L}] = 0$ since \mathbb{L} is composed entirely of projectors onto the same subspaces over which H_s is block-diagonal. The crucial effect of this commutivity is that

$$\rho(t) = e^{\mathbb{H}t + \mathbb{L}t} \{\rho(0)\} = e^{\mathbb{H}t} e^{\mathbb{L}t} \{\rho(0)\} = e^{\mathbb{L}t} e^{\mathbb{H}t} \{\rho(0)\}.$$

Hence the coherent and dissipative contributions to the evolution are independent and can be applied separately.

In the special case where $H_s = H_S$ is a mirror-inverting Hamiltonian this property manifests itself directly in the accumulative noise $\Lambda^{[1]}$. Using the chain as a channel involves initializing it in a spin-polarized state

$$\rho(0) = |\uparrow\rangle \langle \uparrow|_1 \otimes \cdots \otimes \varsigma_j \otimes \cdots \otimes |\uparrow\rangle \langle \uparrow|_{\bar{j}} \otimes \cdots \otimes |\uparrow\rangle \langle \uparrow|_N,$$

aside from the spin j which is in input state ς . If we first apply the coherent evolution for a time τ then, as outlined in section 2, the state becomes

$$\rho_1 = e^{\mathbb{H}\tau} \{\rho(0)\} = |\uparrow\rangle \langle \uparrow|_1 \otimes \cdots \otimes |\uparrow\rangle \langle \uparrow|_j \otimes \cdots \otimes \varsigma_j \otimes \cdots \otimes |\uparrow\rangle \langle \uparrow|_N,$$

where the state ς is transferred to the mirror spin \bar{j} . Since the whole chain is spin-polarized, aside from at spin \bar{j} , the action of the superoperator \mathbb{L} on such a state is completely equivalent to single-spin decay noise at that spin alone. Thus, the final output state φ of spin \bar{j} after tracing out all other spins (denoted as c)

$$\varphi_{\bar{j}} = \text{tr}_c(e^{\mathbb{L}\tau} \{\rho_1\}),$$

is identical, irrespective of $N \nmid$, to the output state for a chain with $N = 1$ where the input state ς is simply exposed to single spin decay noise for a time τ .

7.2.2. Dephasing noise - We find that the behavior of ϵ_{\min} and $\langle F \rangle$, displayed in figure 5(a)-(b), for the accumulative noise of the spin chain with local dephasing rapidly converges with the length of the chain. In particular figure 5(a) shows that the chain does not become entanglement breaking for the wide range of chain lengths N and couplings κ/J investigated. In figure 5(c) we plot the coupling κ_f/J at which the fidelity drops below $\langle F \rangle < 0.99$. This plot indicates that the coupling must not

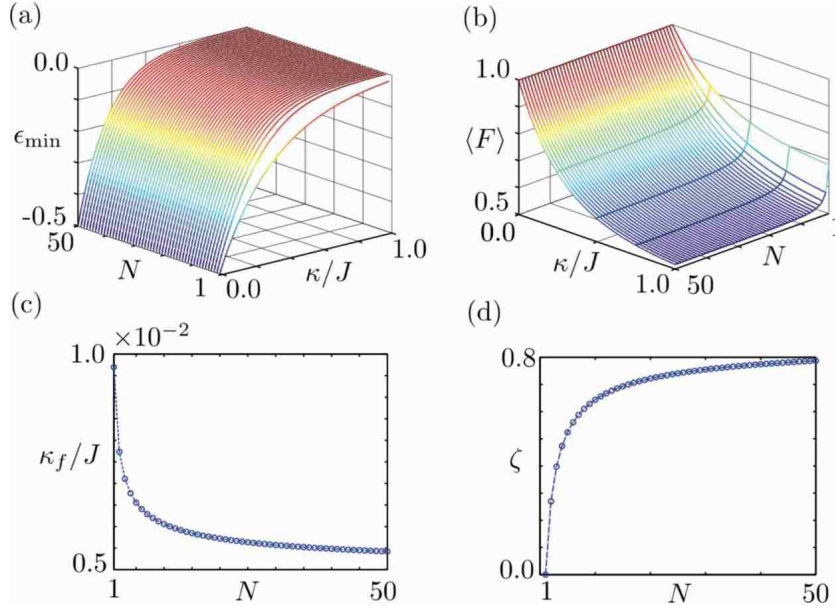


Figure 5. For local dephasing noise - (a) The minimum eigenvalue ϵ_{\min} of the partial transposition of ρ^A and (b) the average fidelity $\langle F \rangle$, both as a function of the chain length N and coupling strength κ/J . (c) The coupling κ_f/J at which the fidelity shown in (b) drops below $\langle F \rangle < 0.99$ against the chain length N . (d) The fit parameter ζ as a function of N .

exceed $\kappa/J = 5 \times 10^{-3}$ for chain lengths of order $N = 50$ for useful fidelities to be achieved.

One might expect that the average fidelity $\langle F \rangle$ can be reproduced by assuming that a single qubit is sent through a purely dephasing channel with a coupling κ dependent on N . However, our numerical calculations show this not to be the case. Instead, we find that $\langle F \rangle$ is fitted extremely well by assuming that the overall noise $\Lambda^{[1]}$ is simultaneously decay and dephasing. This model noise is also never entanglement breaking for finite κ/J . Using the general expression for the noise model in Appendix A we fitted $\langle F \rangle$ for each N to the model noise fidelity with $\gamma = \kappa$ and $\beta = \zeta\kappa$, where ζ is the only fit parameter. The parameter ζ obtained as a function of N is plotted in figure 5(d). It shows that as the chain length increases the decay rate β increases and becomes of the same order as the dephasing rate γ . Intuitively this type of model might be expected to describe the accumulative noise of the chain. Like local decay noise in the section 7.2.1 an initial state with support in $\mathcal{H}_0 \oplus \mathcal{H}_1$ will remain so at all times. However, unlike local decay noise the coherent and dissipative contributions to the projected master equation do not commute and so perfect mirror inversion is not obtained for any $\kappa/J > 0$. As a result the input state on the first spin is never perfectly refocused to the N -th spin causing a ‘leakage’ of the \downarrow population over other spins in the chain. Since the N -th spin is the output qubit at time τ this effect appears as decay noise.

* The Hamiltonian H_S defined in section 2 is one such example.

‡ On the proviso that the inversion time τ is kept constant with N .

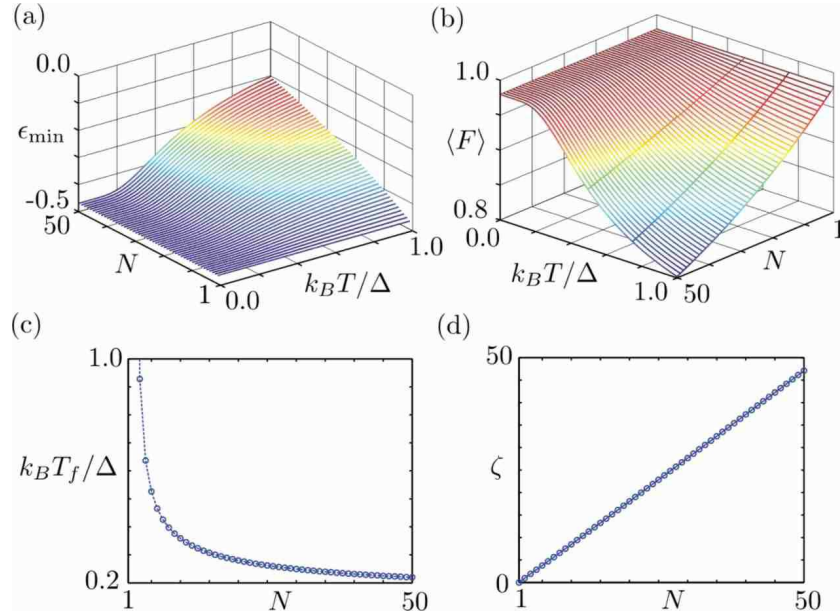


Figure 6. For local thermal reservoirs - (a) The minimum eigenvalue ϵ_{\min} of the partial transposition of ρ^Λ and (b) the average fidelity $\langle F \rangle$, both as a function of the chain length N and temperature T for noise caused by a coupling strength $\kappa/J = 0.02$. (c) The temperature T_f/Δ at which the fidelity shown in (b) drops below 99% of its value at $T = 0$ against the chain length N . (d) The fit parameter ζ as a function of N .

To gauge how accurate the assumed noise model was compared to the actual noise superoperator $\Lambda^{[1]}$ we computed the fidelity [31]

$$F_\Lambda(\rho^\Lambda, \rho_m^\Lambda) = \text{tr} \left(\sqrt{\sqrt{\rho^\Lambda} \rho_m^\Lambda \sqrt{\rho^\Lambda}} \right) \quad (11)$$

between the states ρ^Λ and ρ_m^Λ isomorphic to $\Lambda^{[1]}$ and the model noise, respectively (see Appendix C for details). We find that over all parameters considered the infidelity $1 - F_\Lambda < 3.2 \times 10^{-2}$ which indicates that the model is capturing the accumulative noise of the chain to good approximation.

7.2.3. Thermal noise (finite- T) - For local thermal noise we restrict our consideration to a suitably weak coupling $\kappa/J = 0.02$ so that the corresponding average fidelity at $T = 0$ is $\langle F \rangle = 0.98$ and still sizable. In figure 6(a) ϵ_{\min} is plotted and demonstrates that up to temperatures $T = \Delta$ and chain lengths $N = 50$ the accumulative noise of the chain is not entanglement breaking. The behaviour of both ϵ_{\min} and $\langle F \rangle$ in figure 6(b) indicates that their insensitivity to the chain length N , seen earlier for the $T = 0$ decay noise, persists for temperatures $T < 0.2\Delta$. This is further confirmed by figure 6(c) where the temperature T_f/Δ at which the fidelity drops to 99% of its value at $T = 0$ is above $T = 0.2\Delta$ for chain lengths up to $N = 50$.

In order to reproduce the fidelity surface of figure 6(b) we fitted a noise model in which $\alpha(T)$ and $\beta(T)$ remain unchanged from those in equation (8) but now include a non-zero, temperature-dependent dephasing rate $\gamma(T) = \zeta\alpha(T)$. As a result the

effective noise of the chain is still described by a coupling to thermal reservoir of temperature T . The corresponding fit parameter ζ for each N is shown in figure 6(d) and is seen to be linear and very nearly $\zeta(N) = N$. The accuracy of this model noise compared to the numerically determined noise was found to be extremely good with F_Λ computed via equation (11) giving $1 - F_\Lambda < 3.6 \times 10^{-5}$.

In section 5 we found from equation (10) that for single-qubit thermal noise, with $\gamma = 0$ and acting for a time τ , a coupling $\kappa/J > 0.56$ was required for the channel to become entanglement breaking at $T \rightarrow \infty$. Consequently, a single-qubit channel, with the weak coupling $\kappa/J = 0.02$ chosen, never becomes entanglement breaking at any temperature. Using our model for the accumulative noise of the chain in which a non-zero $\gamma(T) \approx N\alpha(T)$ emerges we have determined an approximate analytical expression for the critical length N_c at which entanglement breaking will occur for a given temperature T and local coupling κ/J as

$$N_c \left(T, \frac{\kappa}{J} \right) \approx \frac{J(1 + e^{-\Delta/T})}{2\kappa\pi e^{-\Delta/T}} \log \left\{ \frac{(1 + e^{-\Delta/T})^2}{2e^{-\Delta/T} [\cosh(\frac{\kappa\pi}{J}) - 1]} \right\}.$$

For any $\kappa > 0$ this function monotonically increases with decreasing T from a finite asymptotic value at $T \rightarrow \infty$ and diverges at $T = 0$. For the weak coupling used in this section the critical length at $T \rightarrow \infty$ is $N_c = 111$ spins.

7.2.4. Depolarizing noise (high- T limit) - For local depolarizing noise we find that the accumulative noise of the chain becomes entanglement breaking at a threshold coupling κ_c/J that reduces with the chain length N as shown in figure 7(a). The fidelity $\langle F \rangle$ shown in figure 7(b) decreases rapidly with κ/J for $N > 5$. The coupling κ_f/J at which the fidelity drops to $\langle F \rangle = 0.99$ is plotted in figure 7(c) and indicates that the condition $\kappa/J < 3 \times 10^{-4}$ has to be fulfilled in order to achieve reasonable fidelities for chain lengths up to $N = 50$. Figure 7(b) also shows that the decay of $\langle F \rangle$ with κ/J changes from an exponential behaviour for small N to a double-exponential behaviour for large N . This indicates that the accumulative noise of the chain does not remain purely depolarizing, however, we do find that it is still well approximated by the class of noise introduced in section 5. Using the noise model with $\alpha = \beta = \zeta_1\kappa$ and $\gamma = \zeta_2\kappa$, and fitting ζ_1 and ζ_2 , the fidelity curves can be accurately reproduced for all parameters considered. By restricting $\alpha = \beta$ this model is still thermal noise in the limit $T \rightarrow \infty$, but importantly we allow the total decay rate to increase from κ and also independently allow the dephasing rate to increase from $\frac{1}{2}\kappa$, both as a function of N . The fitting parameters plotted in figure 7(d) show that ζ_1 increases from its initial value of $\frac{1}{2}$ to a little over unity, whereas ζ_2 displays a linear increase with N becoming nearly 30 times larger than ζ_1 for $N = 50$. To establish the validity of this model we compare it to the actual noise computed numerically by calculating F_Λ via equation (11). We find that $1 - F_\Lambda < 1.5 \times 10^{-2}$.

The dependence of the critical coupling κ_c/J with N is plotted in figure 8 and appears to be described well by a power-law $\kappa_c/J \approx N^{-x}$ with $x = 0.68$. Using the fitted noise model the critical coupling can be obtained by solving a special case of equation (9) of the form

$$[\zeta_1(N)]^2 \exp[2\zeta_2(N)\pi \text{frac}\kappa J] \left\{ \cosh \left[2\zeta_1(N)\pi \frac{\kappa}{J} \right] - 1 \right\} \geq \frac{1}{2},$$

as a function of N using the functions $\zeta_1(N)$ and $\zeta_2(N)$ plotted in figure 7(d). The result of this is also shown in figure 8 and is consistent with a power law with exponent $x = 0.72$.

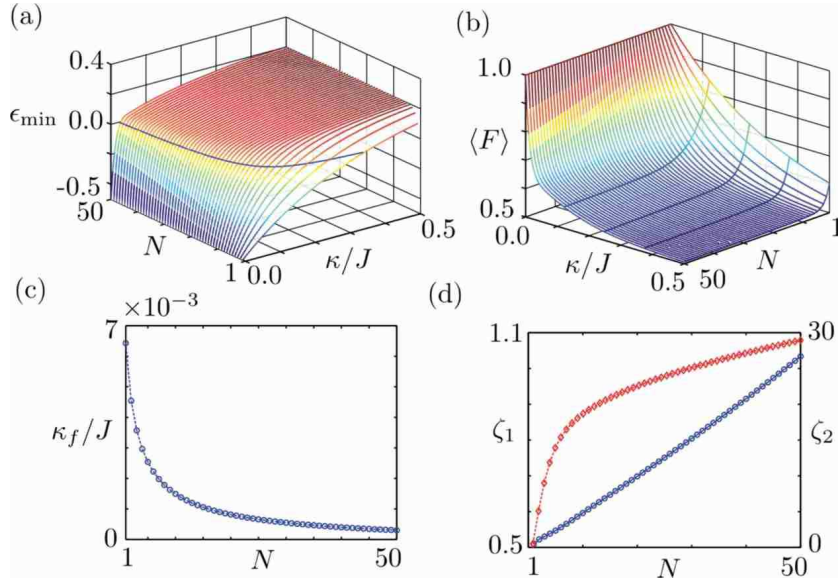


Figure 7. For local depolarizing noise - (a) The minimum eigenvalue ϵ_{\min} of the partial transposition of ρ^Λ and (b) the average fidelity $\langle F \rangle$, both as a function of the chain length N and coupling strength κ/J . The critical coupling κ_c/J for each chain length N at which the accumulative noise is entanglement breaking is given by the intersection with the $\epsilon_{\min} = 0$ plane shown in (a). (c) The coupling κ_f/J at which the fidelity shown in (b) drops below $\langle F \rangle < 0.99$ against the chain length N . (d) The fit parameters ζ_1 (left axis and ‘ \diamond ’) and ζ_2 (right axis and ‘ \circ ’) as a function of N .

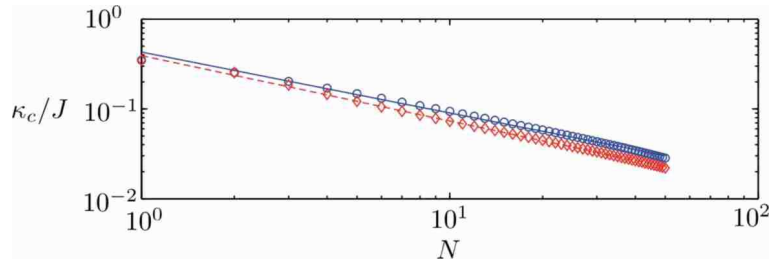


Figure 8. The critical coupling κ_c/J at which the accumulative noise of the chain becomes entanglement breaking as a function of the chain length N on a log-log scale. The numerical data is plotted with ‘ \circ ’ and the fitted power law $\kappa_c/J \approx N^{-x}$ is the solid line with an exponent $x = 0.68$. The solution for the critical coupling of the noise model are plotted with ‘ \diamond ’ and the dotted line is the power law fit with an exponent $x = 0.72$.

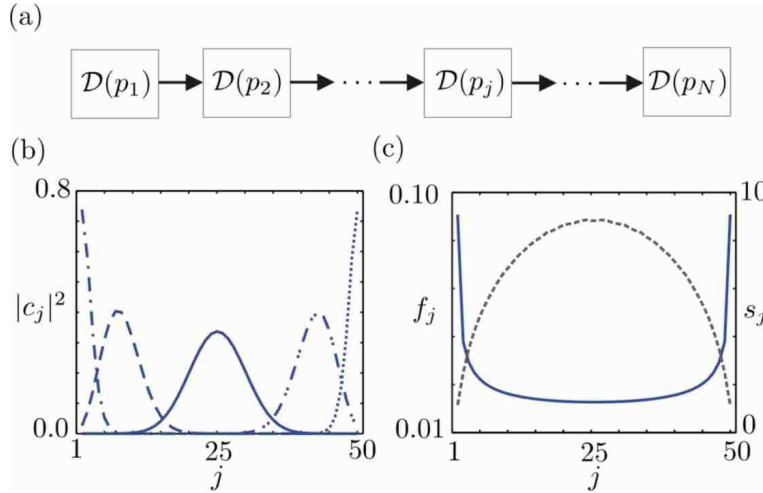


Figure 9. (a) A simple model for state transfer in a mirror inverting chain with local depolarizing noise. Each spin on the chain is considered to be a depolarizing channel $\mathcal{D}_j\{\rho\} = p_j\rho + \frac{1}{2}(1-p_j)\mathbb{1}$ with $p_j = \exp(-\kappa f_j s_j \tau)$. The fraction of the total time τ spent in each channel f_j is approximately proportional to the inverse of the average spin-coupling for the j -th spin. (b) The spin packets probability distribution $|c_j|^2$ in the $|j\rangle$ basis for a selection of times. These are readily computed from the x -axis rotation of z angular momentum states from which the spread s_j can then be extracted. (c) The fraction of time f_j (left axis and solid line) and spread s_j (right axis and dashed line) as a function of the spin j .

To gain a qualitative understanding of the origin of this power-law scaling of κ_c/J with N we consider a simple model of this noise scenario. Specifically we replace each spin of the chain by a depolarizing channel which preserves the input state with probability p_j and where state transfer corresponds to the concatenation of these channels shown in figure 9(a). The accumulative noise of this sequence of single qubit channels is then also a depolarizing channel with probability $p = \prod_j p_j$. In figure 9(b) the progression of a spin packet in the chain resulting from a spin-flip excitation at the first spin is shown for a sequence of times for $N = 50$. With this in mind we take the probabilities for each channel as $p_j = \exp(-\kappa f_j s_j \tau)$ where f_j is the fraction of the inversion time τ the centre of the spin packet spends at spin j , and s_j is the number of sites the spin packet spreads across when it is in the region of spin j . Both these quantities can be readily derived from the properties of angular momentum and are plotted in figure 9(c). From this we see that the spin packet is narrow and slow at the edges while being wide and fast at the centre. The critical coupling for this simple model can be extracted from equation (9) as

$$\frac{\kappa_c}{J} = \frac{\log(3)}{\pi \sum_{j=1}^N f_j s_j}.$$

We find that the competition between the spreading and speed of a spin packet across the chain as a function of its length N naturally gives rise to a power-law dependence for κ_c/J .

7.3. Effective two qubit gate

In this section we consider the EB as a mediator of an effective two-qubit $c\text{-}\sigma^z$ gate. We systematically compute the average gate fidelity $\langle F \rangle$ for this operation and the minimum eigenvalue ε_{\min} of the partial transposition, with respect to the bipartition (12)(34), of the 4 qubit state ϱ^Λ isomorphic to the accumulative noise $\Lambda^{[2]}$. If $\varepsilon_{\min} < 0$ then the noisy operation of the EB is still capable of entanglement generation. We also use the behaviour of $\langle F \rangle$ to determine if the accumulative noise is a product of local noise of the type introduced in section 5.

7.3.1. Decay noise (low- T limit) - Earlier in section 7.2.1 we found that using the EB as a single-qubit channel with local decay noise results in the accumulative noise $\Lambda^{[1]}$ being independent of N . Thus all chain lengths were equivalent to a chain with just one spin. When the EB is used to mediate a $c\text{-}\sigma^z$ gate with local decay noise, our numerical results show that $\langle F \rangle$, for the lengths investigated, is independent on N . However, further investigation reveals that $\Lambda^{[2]}$ itself does possess a weak length dependence demonstrating that this result is a consequence of $\langle F \rangle$ being completely insensitive to these changes. A length dependence of $\Lambda^{[2]}$ is expected since, in contrast to the single-qubit channel in section 7.2.1, the projected master equation in the subspace $\mathcal{H}_0 \oplus \mathcal{H}_1 \oplus \mathcal{H}_2$ does not have commuting coherent and dissipative contributions. Our numerical calculations furthermore indicate that ε_{\min} is weakly length dependent but is never positive over the parameter range and lengths investigated.

We find that the coupling at which the fidelity drops to $\langle F \rangle < 0.99$ is $\kappa_f/J = 4.0 \times 10^{-3}$ independent of N . In addition to the average gate fidelity we also compute the specific gate fidelity F^{++} of the initial state $|++\rangle$ using equation (3) and the numerically determined superoperator $\Lambda^{[2]}$. Using this initial state makes the operation equivalent to the noisy generation of a two-qubit cluster state. We find that the coupling at which this fidelity drops to $F^{++} < 0.99$ is $\kappa_f^{++}/J = 8.5 \times 10^{-3}$, and turns out to be independent of N . Thus, this specific preparation is twice as resilient to decay noise than the average preparation.

7.3.2. Dephasing noise - For local dephasing noise we find that ε_{\min} , shown in figure 10(a), is never positive over the parameter regime considered and therefore the ability to generate entanglement is retained in the presence of this noise. In a similar way to the single-qubit channel fidelity we find that the gate fidelity, plotted in figure 10(b), rapidly converges with increasing N . To understand the nature of the accumulative noise we attempted to fit the fidelity to a model where the ideal two-qubit gate U is implemented and then product noise $\Lambda_{\text{mod}}^{[1]} \otimes \Lambda_{\text{mod}}^{[1]}$ is applied where $\Lambda_{\text{mod}}^{[1]}$ is a single-spin superoperator describing noise from the class introduced in section 5. In fact we found that the best fit was obtained when $\Lambda_{\text{mod}}^{[1]}$ was further restricted to the case used in section 7.2.2 where $\gamma = \kappa$ and $\beta = \zeta\kappa$. The validity of these fits determined from F_Λ had a peak infidelity of $1 - F_\Lambda \approx 0.3$ for strong coupling with $N = 2$ and so the actual noise bears no resemblance to this product model. This rapidly drops to $1 - F_\Lambda \approx 5 \times 10^{-2}$ for larger N , which indicates that the product noise model becomes more valid for longer chains. This behavior is sensible since in long chains the two spin packets do not overlap for the majority of the evolution time τ and therefore experience independent noise during this time. We also find that the coupling at which the fidelities $\langle F \rangle$ and F^{++} drop to 99% are $\kappa_f/J = 2.5 \times 10^{-3}$ and

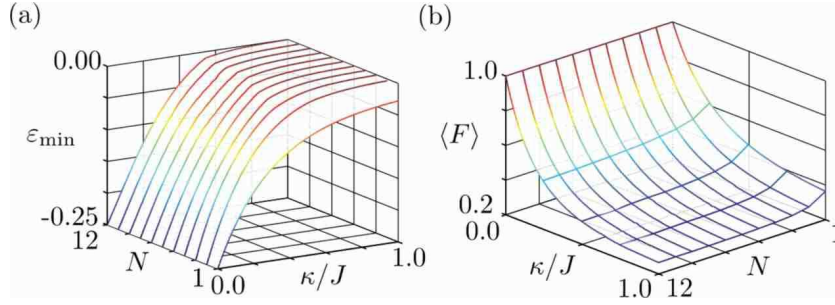


Figure 10. For local dephasing noise - (a) The minimum eigenvalue ε_{\min} of the partial transposition of the 4 qubit mixed state ϱ^Λ for the bipartition (12)(34) and (b) the average gate fidelity $\langle F \rangle$, both as a function of the chain length N and coupling strength κ/J .

$\kappa_f^{++}/J = 6.5 \times 10^{-3}$ respectively, for chain lengths up to $N = 12$.

7.3.3. Thermal noise (finite- T) - For local thermal noise we find that ε_{\min} , shown in figure 11(a), is only marginally increased and remains negative over the parameters we considered. Despite this from our analysis of the single-qubit channel there is good reason to suspect that for longer chains and higher temperatures this noise will generate $\varepsilon_{\min} > 0$. Along with $\langle F \rangle$ depicted in figure 11(b) ε_{\min} has a very weak dependence on N for $T/\Delta < 0.2$ similar to that encountered for a single-qubit channel in section 7.2.3. We again fit the fidelity surface with a product noise model $\Lambda_{\text{mod}}^{[1]}$ assuming the same single spin noise as used in section 7.2.3 where $\alpha(T)$ and $\beta(T)$ remain unchanged from those in equation (8) and $\gamma(T) = \zeta\alpha(T)$ with a fit parameter ζ . This fitting produces a linear dependence of ζ with N as found earlier for the single qubit channel. In this case the infidelity for the product noise model is $1 - F_\Lambda < 2.3 \times 10^{-2}$ and is therefore a good approximation to the accumulative noise over the parameter range investigated. This indicates the noise is very effective at eliminating correlations which might be built up by the dynamics of the chain. We also find that the temperatures at which the fidelities $\langle F \rangle$ and F^{++} drop to 99% of their $T = 0$ value are $T_f/\Delta = 0.29$ and $T_f^{++}/\Delta = 0.34$ respectively, for chain lengths up to $N = 12$.

7.3.4. Depolarizing noise (high- T limit) - For local depolarizing noise we observe in figure 12(a) that ε_{\min} becomes positive for a sizable portion of the parameter range explored. We can therefore only be certain that entanglement generation is possible with the EB outside this region of parameters, i.e. $\kappa/J < 0.15$ for chain lengths up to $N = 12$. The average gate fidelity plotted in figure 12(b) shows that $\kappa \ll J$ is required in order to achieve a reasonable average fidelity. When fitting a product noise model to $\langle F \rangle$ we obtain an infidelity $1 - F_\Lambda < 4.5 \times 10^{-2}$ which decreases significantly with larger coupling κ/J . This is consistent with stronger local noise destroying correlations between the spin packets and therefore decorrelating the noise. We also find that the coupling at which the fidelities $\langle F \rangle$ and F^{++} drop to 99% are $\kappa_f/J = 8.0 \times 10^{-4}$ and $\kappa_f^{++}/J = 1.4 \times 10^{-3}$ respectively, for chain lengths up to $N = 12$.

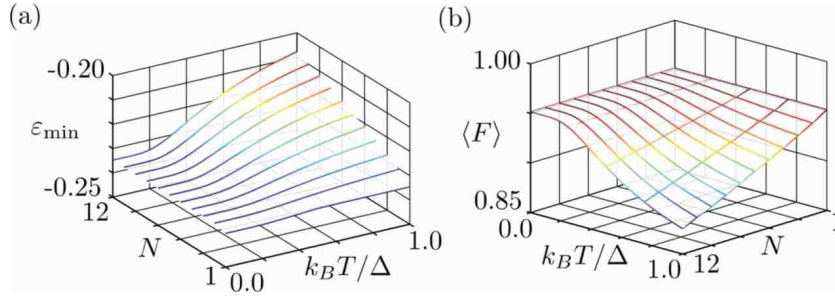


Figure 11. For local thermal reservoirs - (a) The minimum eigenvalue ε_{\min} of the partial transposition of the 4 qubit mixed state ρ^A for the bipartition (12)(34) and (b) the average gate fidelity $\langle F \rangle$, both as a function of the chain length N and temperature $k_B T/\Delta$ using a coupling $\kappa/J = 0.02$

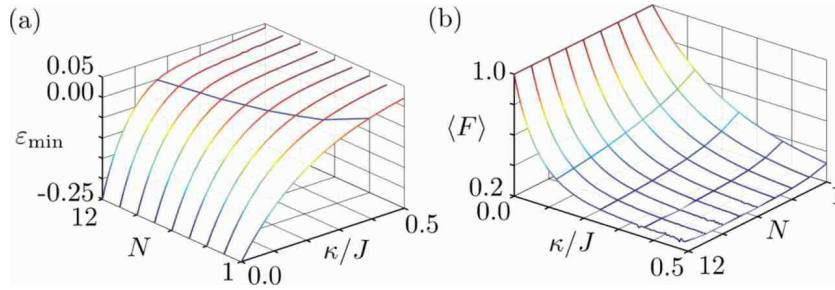


Figure 12. For local depolarizing noise - (a) The minimum eigenvalue ε_{\min} of the partial transposition of the 4 qubit mixed state ρ^A for the bipartition (12)(34) and (b) the average gate fidelity $\langle F \rangle$, both as a function of the chain length N and coupling strength κ/J . The critical coupling κ_c/J for each chain length N at which the entanglement generating capability of the EB is no longer certain is given by the intersection with the $\varepsilon_{\min} = 0$ plane shown in (a).

8. Implications for graph state generation

In section 3 a general scheme for creating arbitrary graph states was outlined which exploits the multi-qubit circuit implemented by the EB. A complete characterization of the influence of noise on the full scheme is beyond the scope of the current work. Here, we instead focus on the most direct implication of the results presented in section 7.3 by investigating graph state generation for five qubits using the EB to mediate a two-qubit $c\text{-}\sigma^z$ only. As an example we focus on the generation of a linear cluster state, shown in figure 13(a), and a GHZ state, shown in figure 13(b), under the influence of local dephasing noise. These two states were chosen because they have the same number of edges but very different topologies.

The generation protocol begins by initializing the first five qubits of a ten qubit register in the state $|+\rangle$. For the previous calculations in section 7.3 the input and output qubits were exclusively the end spins in the EB. For graph state generation, however, each usage of the EB to establish an edge will necessarily involve using different spins of the chain as the input qubits (as well as output qubits). Our numerical calculations indicate that the superoperator $\Lambda^{[2]}$ does depend weakly on

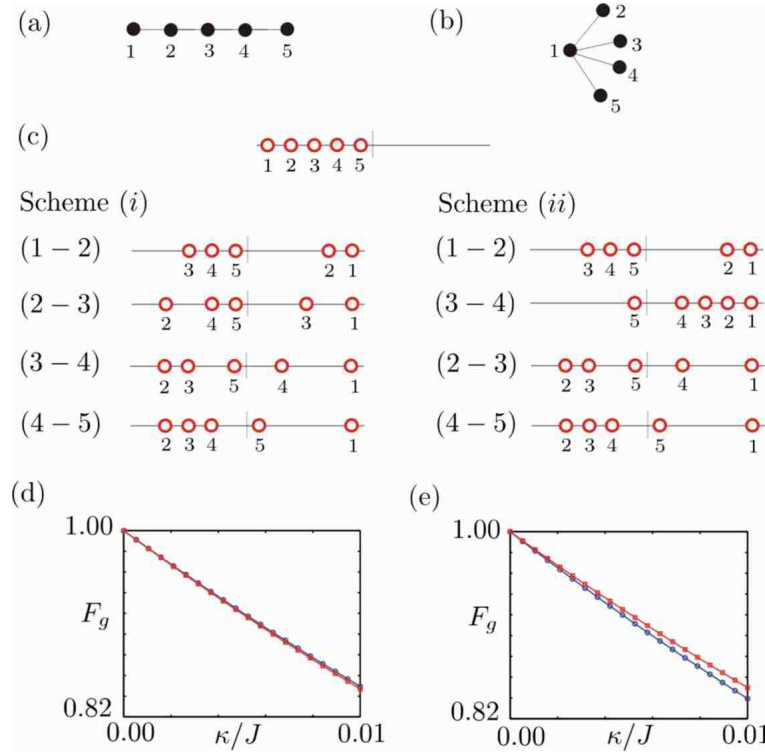


Figure 13. We consider the generation of (a) the linear cluster state and (b) the GHZ state for five qubits. The qubits representing the graph vertices are initialized in the first half of the register as shown in (c). Two schemes for the sequence in which the EB is used to mediate the necessary two-qubit gates are investigated. Scheme (i) proceeds with the gates in a sequential order, while scheme (ii) proceeds by performing gates between qubits which are closest in the register at a given step. For the linear cluster state the two schemes are explicitly shown in (c). In (d) the graph state fidelity F_g for the linear cluster state (‘ \circ ’) and GHZ state (‘ \square ’) constructed with scheme (i) is plotted, and in (e) the same is shown for scheme (ii).

the input qubit locations. For this reason the order in which the gates are performed will affect the quality of the overall state. To illustrate effect this we computed the graph state generation protocol for two different gate ordering schemes. The first, scheme (i), performs the necessary gates in a simple sequential order according to the qubit labels. The second, scheme (ii), performs a gate between qubits, from the list of edges to be established, which are closest in the register at a given step (which is often not unique). These two schemes are shown explicitly for the linear cluster state in figure 13(c). We computed numerically the superoperator $\Lambda^{[2]}$ for all input locations required for these two schemes to generate the linear cluster state and the GHZ state. By concatenating the appropriate noisy gates in the specified order the imperfect graph state was obtained.

For scheme (i), shown in figure 13(d), we find that the linear cluster state fidelity F_g is slightly above that for the GHZ state with them having a fidelity greater than 99% for $\kappa/J < 5.7 \times 10^{-4}$ and $\kappa/J < 6.0 \times 10^{-4}$, respectively. For scheme (ii), shown

in figure 13(e), the GHZ state fidelity is virtually unchanged from that of scheme (i), whereas the linear cluster state fidelity has dropped below that of the GHZ state giving a slightly reduced $\kappa/J < 6.1 \times 10^{-4}$ for a fidelity greater than 99% to be attained. The average gate fidelity for a $N = 10$ chain, computed in section 7.3 using the end spins as the input qubits, drops to 99% when $\kappa/J < 2.6 \times 10^{-3}$ for local dephasing noise. Thus the noise tolerance for the generation of these graph states is reduced by a factor of approximately 4.5 in comparison. Additionally, the results appear to indicate that only a weak change in the fidelity is observed with the graph topology and input qubit locations for a $N = 10$ chain. Further work is need to confirm if this insensitivity is maintained for more varied topologies over larger numbers of vertices and longer chains.

These preliminary results give a clear indication of useful directions for future work. This includes studying the dependence of the EB on the input qubit locations with different noise models as well as chain lengths and determining wether there is any generic behaviour. For the full graph state generation scheme of section 3 the quality of the multi-qubit circuits implemented by the EB with noise needs to be studied along with their likely dependence on the input qubit locations. This may well reveal a trade-off between using the EB less times with more qubits or more times with fewer qubits. With this information and for a given graph topology, the graph state generation scheme under the influence of noise could be optimized, in terms of the sequence and type of gates implemented.

9. Conclusion

In summary we have investigated the influence of local noise on the mirror inverting EB spin chain. For the case where the EB is utilized as a single qubit channel we have found that the accumulative noise of the EB for local decay noise is independent of its length N and explained this unexpected behaviour. Additionally, we have found that neither local decay nor dephasing noise cause the EB to become entanglement breaking, in contrast to local thermal and depolarizing noise. For the latter two cases we have determined the critical length N_c and critical coupling κ_c/J at which entanglement breaking occurs, respectively. The local depolarizing noise κ_c/J is found to exhibit a power-law dependence on N which is explained by the competition between the speed and spreading of the spin packet in the EB.

For the case where the EB is used to mediate an entangling $c\text{-}\sigma^z$ gate we find that the entanglement generating capability of the EB is never lost in presence of local decay or dephasing noise. For local dephasing noise the resulting operation of the EB becomes progressively closer to product noise with increasing N . Both local thermal and depolarizing noise are well approximated by product noise models due to the severity at which they decohere the spin chain. For local depolarizing noise our results indicate that the entanglement generating capability of the EB can only be guaranteed for couplings $\kappa/J < 0.15$ for chain lengths up to $N = 12$.

We have also performed a preliminary analysis of the graph state generation scheme which uses the EB, with local dephasing noise, to individually implement the necessary $c\text{-}\sigma^z$ gates for a five qubit graph state. As an example we focussed on the linear cluster state and GHZ state. As expected we found that the concatenation of these operations reduces the tolerance to noise. In this case the reduction was by a factor of approximately 4.5 for both states compared to the average fidelity of a single gate. More work is needed to determine how this behaviour scales for larger graph

states constructed with longer EB chains. Finally, we note that while our results indicate that there are tight constraints on the levels of tolerable noise for graph state generation this can be weakened within the framework of one-way quantum computing due to the separation between the preparation and consumption of entanglement [39]. In principle this enables the resulting noisy graph states to be purified prior to their use [40, 41].

Acknowledgments

SRC thanks Richard Walters for helpful discussions. This work is supported by the UK EPSRC through QIP IRC (GR/S82176/01) and project EP/C51933/1, the Berrow Scholarship (MB), and the Keble Association (AK).

Appendix A. Limits of the local noise model

In section 5 the general form for the Kraus operators was given in equation (7) for the noise model considered here. Since the expressions for the general matrix elements Υ_i of the diagonal operators are rather lengthy we have postponed their introduction to this appendix. To begin with the following quantities are defined [7]

$$\begin{aligned}\lambda_0(t) &= \frac{1}{4}[1 + 2e^{-\frac{1}{2}(\alpha+\beta+2\gamma)t} + e^{-(\alpha+\beta)t}], \\ \lambda_1(t) &= \lambda_2(t) = \frac{1}{4}[1 - e^{-(\alpha+\beta)t}], \\ \lambda_3(t) &= \frac{1}{4}[1 - 2e^{-\frac{1}{2}(\alpha+\beta+2\gamma)t} + e^{-(\alpha+\beta)t}], \\ \mu(t) &= \frac{\langle \sigma_z \rangle_s}{4}[1 - e^{-(\alpha+\beta)t}],\end{aligned}$$

using the definitions from section 5. We then find that for $\mu \neq 0$

$$\begin{aligned}\Upsilon_1 &= \frac{1}{2}(x - 2\mu - \lambda_0 + \lambda_3)\sqrt{\frac{\lambda_0 + \lambda_3 - x}{4\mu^2 - (\lambda_0 - \lambda_3)(x - \lambda_0 + \lambda_3)}} \\ \Upsilon_2 &= \frac{1}{2}(2\mu + x - \lambda_0 + \lambda_3)\sqrt{\frac{\lambda_0 + \lambda_3 - x}{4\mu^2 - (\lambda_0 - \lambda_3)(x - \lambda_0 + \lambda_3)}} \\ \Upsilon_3 &= \frac{1}{2}(2\mu + x + \lambda_0 - \lambda_3)\sqrt{\frac{x + \lambda_0 + \lambda_3}{4\mu^2 + (\lambda_0 - \lambda_3)(x + \lambda_0 - \lambda_3)}} \\ \Upsilon_4 &= \frac{1}{2}(x - 2\mu + \lambda_0 - \lambda_3)\sqrt{\frac{x + \lambda_0 + \lambda_3}{4\mu^2 + (\lambda_0 - \lambda_3)(x + \lambda_0 - \lambda_3)}}\end{aligned}$$

making one further definition $x = \sqrt{4\mu^2 + (\lambda_0 - \lambda_3)^2}$. As expected the Kraus operators in equation (7) simplify considerably for a number of important special cases. In particular for $\mu = 0$ the Kraus operators become $E_1 = \sqrt{\lambda_0} \mathbb{1}$, $E_2 = \sqrt{\lambda_1} \sigma^x$, $E_3 = \sqrt{\lambda_2} \sigma^y$, $E_4 = \sqrt{\lambda_3} \sigma^z$. For $\beta = \kappa$ and $\alpha = \gamma = 0$ they reduce to

$$E_1 = \begin{pmatrix} 1 & 0 \\ 0 & \sqrt{p_1} \end{pmatrix}, \quad E_2 = \begin{pmatrix} 0 & \sqrt{1-p_1} \\ 0 & 0 \end{pmatrix},$$

with $p_1 = e^{-\kappa t}$ describing pure decay noise; for $\gamma = \kappa$ and $\alpha = \beta = 0$ they reduce to $E_1 = \sqrt{p_2} \mathbb{1}$, $E_2 = \sqrt{1-p_2} \sigma^z$ with $p_2 = \sqrt{\frac{1}{2}(1 + e^{-\kappa t})}$ describing pure dephasing;

while for $\alpha = \beta = \gamma = \frac{1}{2}\kappa$ they become $E_1 = \sqrt{1-3p_3} \mathbb{1}$, $E_2 = \sqrt{p_3} \sigma^x$, $E_3 = \sqrt{p_3} \sigma^y$, $E_4 = \sqrt{p_3} \sigma^z$ with $p_3 = \frac{1}{4}(1 - e^{-\kappa t})$ describing depolarizing noise [31]. For finite- T noise with $\gamma = 0$ and $\alpha + \beta = \kappa$ the Kraus operators take the form

$$E_1 = \sqrt{P_\uparrow} \begin{pmatrix} 1 & 0 \\ 0 & \sqrt{e^{-\kappa t}} \end{pmatrix}, \quad E_2 = \sqrt{P_\uparrow} \begin{pmatrix} 0 & \sqrt{1 - e^{-\kappa t}} \\ 0 & 0 \end{pmatrix},$$

$$E_3 = \sqrt{P_\downarrow} \begin{pmatrix} \sqrt{e^{-\kappa t}} & 0 \\ 0 & 1 \end{pmatrix}, \quad E_4 = \sqrt{P_\downarrow} \begin{pmatrix} 0 & 0 \\ \sqrt{1 - e^{-\kappa t}} & 0 \end{pmatrix}.$$

For $\mu \neq 0$ the average fidelity for a single-qubit channel experiencing this class of noise can be computed from equation (4) as

$$\langle F \rangle = \frac{1}{6} \left(2 + \frac{(\lambda_0 - \lambda_3 + x)^2 (\lambda_0 + \lambda_3 + x)}{4\mu^2 + (\lambda_0 - \lambda_3)(\lambda_0 - \lambda_3 + x)} + \frac{(\lambda_0 - \lambda_3 - x)^2 |\lambda_0 + \lambda_3 - x|}{|4\mu^2 - (\lambda_0 - \lambda_3)(\lambda_3 - \lambda_0 + x)|} \right).$$

For finite- T noise with $\gamma = 0$ this equation reduces to

$$\langle F_T \rangle = \frac{1}{2} + \frac{1}{3} e^{-\frac{1}{2}\kappa t} + \frac{1}{6} e^{-\kappa t},$$

and has a double exponential decay independent of T making it equally applicable to the $T = 0$ decay channel. For the special case where $\mu = 0$ the expression for $\langle F \rangle$ dramatically simplifies to

$$\langle F_{\mu=0} \rangle = \frac{1}{6} (4\lambda_0 + 2),$$

from which the well known fidelities [31] for dephasing and depolarizing channels can easily be evaluated as

$$\langle F_{\text{dephase}} \rangle = \frac{2}{3} + \frac{1}{3} e^{-\kappa t},$$

$$\langle F_{\text{depolar}} \rangle = \frac{1}{2} + \frac{1}{2} e^{-\kappa t},$$

which exponentially decay to $\frac{2}{3}$ and $\frac{1}{2}$, respectively.

Appendix B. Positive partial transposition criterion

Detecting the presence of entanglement in a general bipartite mixed state can be achieved to an extent through the use of the positive partial transposition (PPT) criterion [34, 35]. For an operator O acting on the Hilbert space $\mathcal{H} = \mathbb{C}^{\mathfrak{d}_a} \otimes \mathbb{C}^{\mathfrak{d}_b}$ of two systems a and b the partial transpose with respect to system a is defined as

$$O^{T_a} = \sum_{ij=1}^{\mathfrak{d}_a} \sum_{mn=1}^{\mathfrak{d}_b} \langle i, m | O | j, n \rangle | j, m \rangle \langle i, n |,$$

in terms of some basis $\{|i, m\rangle \mid i = 1, \dots, \mathfrak{d}_a, m = 1, \dots, \mathfrak{d}_b\}$ of \mathcal{H} . Although this definition is basis-dependent the spectrum of O^{T_a} is not. Note also that while the transposition of the full system ab preserves the positivity of the full density matrix $(\rho^{T_a})^{T_b} = \rho^T \geq 0$, in general the transposition with respect to any subsystem does not, and so the partial transpose is not a completely positive operation.

A state ρ of the system ab is separable if and only if it can be expressed as a convex combination of product states

$$\rho = \sum_{i=1}^{\chi} p_i \rho_i^a \otimes \rho_i^b,$$

with $p_i \geq 0$ and $\sum_{i=1}^X p_i = 1$. The PPT criterion then states that $\rho^{T_a} \geq 0$ is a necessary condition for separability of any $d_a \times d_b$ systems. Importantly for 2×2 and 2×3 systems the PPT criterion is necessary and sufficient for separability [34, 35].

Appendix C. Jamiolkowski isomorphism

In section 4 extensive use of the Jamiolkowski isomorphism [36, 7] is made. This isomorphism establishes an equivalence between quantum states and superoperators. To begin suppose we have a type of subsystem S with Hilbert space \mathcal{H} of dimension d and spanned by basis states $\{|i\rangle \mid i = 0, \dots, d-1\}$. For such a subsystem any density operator ρ can be expanded in the operator basis $\{|i\rangle\langle j| \mid i, j = 0, \dots, d-1\}$ with its corresponding matrix elements contained in a d^2 -dimensional vector ρ_{ij} . Superoperators are defined as linear, trace-preserving, completely positive maps of density operators to density operators. Consequently, a superoperator $\Lambda^{[1]}$ acting on a subsystem S is completely described by a $d^2 \times d^2$ super-matrix with elements in the operator basis $\Lambda_{ij,kl}^{[1]}$ as

$$\Lambda^{[1]}\{|i\rangle\langle j|\} = \sum_{kl=0}^{d-1} \Lambda_{ij,kl}^{[1]} |k\rangle\langle l|.$$

This information can be mapped to a quantum state by using two copies a and b of the subsystem S initially prepared in the maximally entangled state $|\Psi\rangle = \frac{1}{\sqrt{d}} \sum_{i=0}^{d-1} |i\rangle \otimes |i\rangle$ and applying the superoperator $\Lambda^{[1]}$ to b as

$$(\mathbb{1} \otimes \Lambda^{[1]})\{|\Psi\rangle\langle\Psi|\} = \frac{1}{d} \sum_{ij=0}^{d-1} |i\rangle\langle j| \otimes \Lambda^{[1]}\{|i\rangle\langle j|\} = \rho^\Lambda,$$

as shown in figure 3(a). The resulting density operator ρ^Λ for the two S subsystems then completely describes $\Lambda^{[1]}$ by containing all of its operator matrix elements $\Lambda^{[1]}\{|i\rangle\langle j|\}$. This can then be used to compute $\Lambda^{[1]}\{\rho^{\text{in}}\} = \rho^{\text{out}}$ on any state ρ^{out} via

$$\Lambda^{[1]}\{\rho^{\text{in}}\} = d \sum_{ij=0}^{d-1} \left(\sum_{kl=0}^{d-1} \rho_{kl}^{\text{in}} \rho_{ki,lj}^\Lambda \right) |i\rangle\langle j| = \rho^{\text{out}},$$

thereby giving the inverse isomorphism.

For a superoperator $\Lambda^{[2]}$ acting on two S subsystems the Jamiolkowski isomorphism proceeds in an analogous way by applying $\Lambda^{[2]}$ on one half of two maximally entangled pairs of subsystems with the setup depicted in figure 3(b) as

$$(\mathbb{1}_a \otimes \Lambda_{bc}^{[2]} \otimes \mathbb{1}_d)\{|\Psi\rangle\langle\Psi|_{ab} \otimes |\Psi\rangle\langle\Psi|_{cd}\} = \varrho^\Lambda.$$

The resulting density matrix ϱ^Λ for the four S subsystems is then

$$\varrho^\Lambda = \frac{1}{d^2} \sum_{ijkl=0}^{d-1} |i\rangle\langle j| \otimes \Lambda^{[2]}\{|ik\rangle\langle jl|\} \otimes |k\rangle\langle l|,$$

and again completely describes $\Lambda^{[2]}$ through its matrix elements in the operator basis of two subsystems.

References

- [1] Jozsa R and Linden N 2003 *Proc. R. Soc. A* **459** 2011
- [2] Vidal G 2003 *Phys. Rev. Lett.* **91** 147902
- [3] Raussendorf R and Briegel H J 2001 *Phys. Rev. Lett.* **86** 5188
- [4] Raussendorf R, Browne D E and Briegel H J 2003 *Phys. Rev. A* **68** 022312
- [5] Hein M, Eisert J and Briegel H J 2004 *Phys. Rev. A* **69** 062311
- [6] Hein M, Dür W, Eisert J, Raussendorf R, Van den Nest M and Briegel H J 2006 (*Preprint quant-ph/0602096*)
- [7] Hein M, Dür W and Briegel H J 2005 *Phys. Rev. A* **71** 032350
- [8] Briegel H J and Raussendorf R 2001 *Phys. Rev. Lett.* **86** 910
- [9] Gottesman D 1997 (*Preprint quant-ph/9705052*)
- [10] Browne D E and Rudolph T 2005 *Phys. Rev. Lett.* **95** 010501
- [11] Walther P, Resch K J, Rudolph T, Schenck E, Weinfurter H, Vedral V, Aspelmeyer M and Zeilinger A 2005 *Nature* **434** 169
- [12] Barrett S D and Kok P 2005 *Phys. Rev. A* **71** 060310(R)
- [13] Bartlett S D and Rudolph T 2006 *Phys. Rev. A* **74** 040302(R)
- [14] Christandl M, Datta N, Ekert A and Landahl A J 2004 *Phys. Rev. Lett.* **92** 187902
- [15] Christandl M, Datta N, Dorlas T C, Ekert A, Kay A and Landahl A J 2005 *Phys. Rev. A* **71** 032312
- [16] Cook R J and Shore B W 1979 *Phys. Rev. A* **20** 539
- [17] Yung M H and Bose S 2005 *Phys. Rev. A* **71** 032310
- [18] Karbach P and Stolze J 2005 *Phys. Rev. A* **72** 030301(R)
- [19] Yung M H 2006 *Phys. Rev. A* **74** 030303
- [20] Kay A 2007 *Phys. Rev. Lett.* **98** 010501
- [21] Clark S R, Moura Alves C and Jaksch D 2005 *New Journal of Physics* **7** 124
- [22] Breuer H P and Petruccione F 2002 *The theory of open quantum systems* 1st ed (Oxford: Oxford University Press)
- [23] Chiara G D, Rossini D, Montangero S and Fazio R 2005 *Phys. Rev. A* **72** 012323
- [24] Cai J M, Zhou Z W and Guo G C 2006 *Phys. Rev. A* **74** 022328
- [25] Burgarth D and Bose S 2006 *Phys. Rev. A* **73** 062321
- [26] Zhou L, Lu J, Shi T and Sun C P 2006 (*Preprint quant-ph/0608135*)
- [27] Briegel H J and Englert B G 1993 *Phys. Rev. A* **47** 3311
- [28] Sachdev S 1999 *Quantum Phase Transitions* 1st ed (Cambridge: Cambridge University Press)
- [29] Plenio M B, Hartley J and Eisert J 2004 *New J. Phys.* **6** 36
- [30] Chaichian M and Hagedorn R 1998 *Symmetries in Quantum Mechanics* 1st ed (London: Institute of Physics)
- [31] Nielsen M and Chuang I L 2000 *Quantum Computation and Quantum Information* 1st ed (Cambridge: Cambridge University Press)
- [32] Dankert C 2005 (*Preprint quant-ph/0512217*)
- [33] Pedersen L H, Mølmer K and Møller N M 2007 (*Preprint quant-ph/0701138*)
- [34] Peres A 1996 *Phys. Rev. Lett.* **77** 1413
- [35] Horodecki M, Horodecki P and Horodecki R 1996 *Phys. Lett. A* **223** 1
- [36] Jamiolkowski A 1972 *Rep. Math. Phys.* **3** 275
- [37] Zwolak M and Vidal G 2004 *Phys. Rev. Lett.* **93** 207205
- [38] Vidal G 2004 *Phys. Rev. Lett.* **93** 040502
- [39] Tame M S, Paternostro M, Kim M S and Vedral V 2005 *Phys. Rev. A* **72** 012319
- [40] Dür W, Aschauer H and Briegel H J 2003 *Phys. Rev. Lett.* **91** 107903
- [41] Aschauer H, Dür W and Briegel H J 2005 *Phys. Rev. A* **71** 012319